Journal of Vacuum Science & Technology B

JVST B

Second Series
Volume 20, Number 6
November/December 2002

Microelectronics and Nanometer Structures

Processing, Measurement, and Phenomena

Papers from the
46th International Conference
on Electron, Ion, and Photon Beam
Technology and Nanofabrication

Papers from the
Third Low Energy Electron
Microscopy/Photoemission
Electron Microscopy Workshop

An official journal of AVS
Published by the Society
Through the American Institute of Physics

Graphitization of Fe-doped amorphous carbon pillars grown by focused-ion-beam-induced chemical-vapor deposition

J. Fujita, M. Ishida, T. Ichihashi, and Y. Ochiai
NEC Fundamental Research Laboratories, 34 Miyukigaoka, Tsukuba 305-8501, Japan

T. Kaito
Seiko Instruments Inc., 36-1 Takenoshita, Oyama, Shizuoka 410-1393, Japan

S. Matsui
Himeji Institute of Technology, 1479-6 Kaneidetchi, Akogun, Hyogo 678-1201, Japan

(Received 28 May 2002; accepted 9 September 2002)

Graphitization of amorphous carbon pillar grown by focused-ion-beam-induced chemical-vapor deposition was demonstrated using an iron catalyst. The graphitization was induced by iron particles at the top of the pillar that were locally doped. Such graphitization of amorphous carbon seems to be based on solid phase crystallization, where homo-epitaxial growth on a graphite template appeared to have occurred. The original three-dimensional shape of an as-grown structure survived solid phase graphitization at 820 °C. © *2002 American Vacuum Society.*
[DOI: 10.1116/1.1518022]

I. INTRODUCTION

Recent progress in the development of stable liquid-ion sources in conjunction with the introduction of a design for an ion optic column has enabled the realization of a fine, 7 nm ion beam. Based on this beam technology, the focused-ion-beam-induced chemical-vapor deposition (FIB-CVD) technique has a big advantage when used in the fabrication of three-dimensional nanostructures.[1-3] Specifically, the penetration depth of an ion and the dispersion length of a secondary electron determine the minimum feature size of the deposited materials to be on the order of several tens of nanometers. However, the beam-induced deposition technique has good controllability in terms of the position, size, and shape to be formed. Even when the target shape contains an overhanging structure, such as a Y branch, the short penetration depth of the ion helps to confine the reactive area of deposition without the accumulation of extra residues around the structure. Such freedom of shape and position controllability is useful for nanomechanics.

However, the carbon nanotube has recently emerged as the most interesting material for application to nanoelectronics. In particular, the energy gap of the single-wall nanotube can be changed with changes of the radii at a certain chirality.[4] Many researchers worldwide have reported demonstrations of field-effect transistors comprised of a nanotube.[5,6] However, it is apparent that the integration of nanotube electronic devices into silicon circuit needs further breakthroughs in control of both the position and size of the radii. Problems such as this are mainly due to the synthesis that occurs in nanotubes, which are generally produced as a random mixture of fibers having different radii, different lengths, bundles, and single- or multi-wall tubes. Therefore, the device fabrication process requires an enormous effort to be expended for the selection of certain nanotube radii and to manipulate the radii to a certain position.

From this viewpoint, the graphitization of an amorphous carbon pillar grown by FIB-CVD may give a promising solution for such applications, if the amorphous pillar can be crystallized without any changes in its original shape. When a hydrocarbon precursor is used in the FIB-CVD process, the as-grown material is constructed by the amorphous carbon containing Ga that comes from the source ion. We previously reported[2] that the annealing of an amorphous carbon pillar in vacuum produced Ga droplets at the surface, and finally these segregated Ga were vaporized at 600 °C. However, the amorphous carbon never became crystallized at temperatures up to 820 °C. However, it is well known that the graphitized temperature in gas-phase production can be reduced by adding small catalyst-like particles of iron. In this article, we will report the results of our study of solid phase graphitization originating from the mother material of FIB-CVD amorphous carbon.

II. PREPARATION OF Fe-DOPED PILLAR

Fe-doped amorphous carbon was grown using two gas sources: phenanthrene for amorphous carbon and ferrocene for Fe. Our FIB system was equipped with two crucibles of source gas, and a two-gas nozzle was directed at the beam point on the substrate, as shown in Fig. 1. The FIB system used was the SEIKO SMI-2050 system. By using the system, Ga ions accelerated at 30 KeV can be focused within a 7 nm beam spot at an ion current of 1 pA. The typical heating temperature of the source crucibles was 50 °C for the ferrocene and 70 °C for the phenanthrene. The base pressure of our FIB system was about 5×10^{-7} Torr, and the averaged gas pressure in the FIB specimen chamber was 5×10^{-5} Torr for the ferrocene, and 7×10^{-7} Torr for the phenanthrene. A typical growth speed of ~10 μm/min was obtained with 1 pA of ion current. The growth speed of the amorphous pillar sensitively depended on the local gas pressure.[1,2] In particular, local deviation of the gas pressure frequently resulted in some deformation of the pillar shapes.

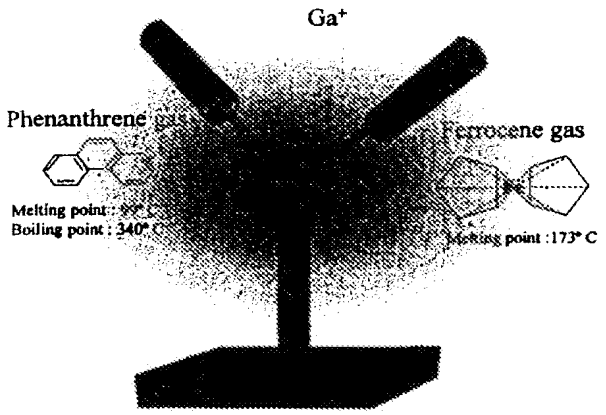

FIG. 1. Schematic diagram of the FIB-CVD system.

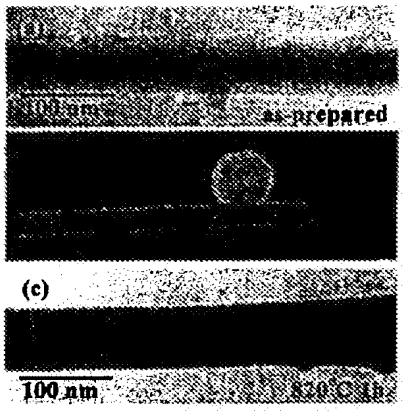

FIG. 2. TEM and SEM images of annealed carbon pillar without Fe.

The pillars tended to bend toward the nozzle. In order to avoid such deformation of the samples, we used a gas reflector. The cleaved surface of a small Si chip stacked on the substrate worked well as a cheap and easy to use reflector. The beam point was adjusted to occupy a space about 50 μm from the reflecting wall. Thus, the CVD sample was surrounded by the primary source-gas jet and the reflected gas in this alignment. This type of geometrical arrangement is also useful for increasing the local gas pressure.

In this experiment, we prepared several types of Fe-doped pillars and Y branches. A uniformly Fe-doped pillar was grown by using a single gas source of ferrocene. Ferrocene ($FeC_{10}H_{10}$) contains 10 at. % of iron against carbon, thus, the majority of the CVD pillar was constructed of amorphous carbon, and the iron seemed to be uniquely dispersed into the amorphous carbon. The CVD pillar grown by ferrocene tended to produce many small spikes around the body.

In contrast, the growth of partial Fe-doped pillars needed two or more production steps; the first growth step of the lower amorphous carbon pillar was followed by the growth of the Fe-doped node. There, the gas changing process needed an intermediate termination of beam emission as well as a change of the stage position. However, the good stability of the beam and the stage system in the FIB system enabled the joining pillars to have good position reproducibility. The Fe-doped region was typically 100 nm long.

III. ANNEALING

Figure 2 shows scanning electron microscopy (SEM) and transmission electron microscopy (TEM) images of annealed amorphous carbon pillars without Fe. The amorphous pillars grown by FIB-CVD contained a certain amount of Ga that came from the ion source. Due to the penetration depth of the 30 KeV Ga ions, this Ga became condensed in the core region of the pillar that was about 40 nm in diameter, which can be seen in Fig. 2 as the central dark area. The condensed Ga seemed to form small particles having diameters of 5–10 nm. After 1 h annealing at 400 °C, the Ga segregated again to form droplets at the surface, as shown in Fig. 2(b). This Ga was completely vaporized at 600 °C, however no crystallization was observed even if the annealing temperature was raised to 820 °C.

In contrast, the existence of Fe particles strongly enhanced the graphitization of the amorphous carbon pillars. Figure 3 shows the TEM images that reveal the graphitization of the uniformly Fe-doped pillars. The Fe seemed to distribute uniformly in the as-grown sample as shown in Fig. 3(a), where the doped iron that appeared in contrast to the darkness extended the entire length of the sample, in comparison with the bright image obtained of the as-grown sample without Fe shown in Fig. 2(a). Such uniformly distributed Fe then cohered into particles, as seen in Fig. 3(b). Local graphitization also occurred around the Fe particles. Two or three layers of graphite sheet surrounded the iron particles, whose structure was very similar to that of a graphite onion.[7] Increasing the annealing temperature caused the Fe particles to grow larger and they tended to concentrate at the central core region of the pillar. The graphitization of the uniformly Fe-doped pillar seemed to progress from the cen-

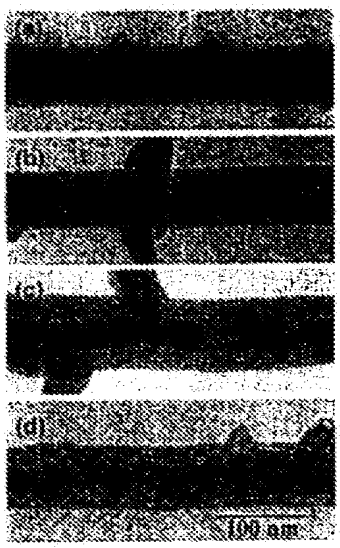

FIG. 3. TEM images of annealed carbon pillar with Fe catalyst.

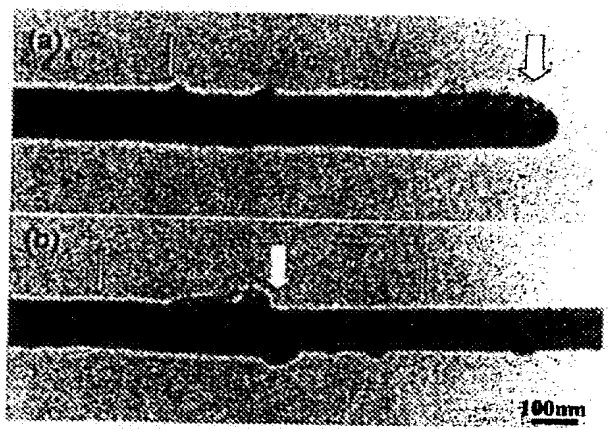

FIG. 4. TEM images of annealed carbon pillar with partial Fe doping. Thick arrows indicated the Fe-doped positions, and thin arrows indicated the front of the graphite.

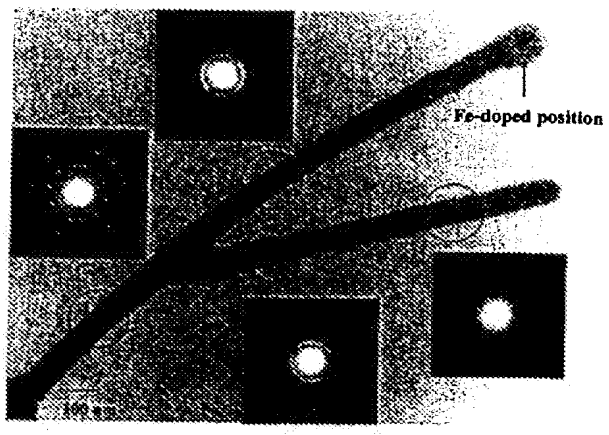

FIG. 5. TEM image of annealed Y-branch pillar.

tral core to the outer shell. Figure 3(c) shows one of the obtained TEM images that clearly indicates the boundaries between the graphite region and the amorphous region. Graphitization extended the entire length of the pillar at 820 °C, as shown in Fig. 3(d). Such solid phase graphitization did not form a single crystal of the pillar, but it did form multi-domain structures having randomly jumbled boundaries.

IV. GRAPHITIZATION OF LOCALLY Fe-DOPED PILLARS

We found that the graphitization of an amorphous carbon pillar can proceed from an iron catalyst at the end of the pillar that is locally doped. Figure 4 shows TEM images of graphitized pillars that had been locally doped with iron. We tested two types of local doping; one formed a doping area at the end of the pillar [Fig. 4(a)] and the other formed one at the middle of the pillar [Fig. 4(b)]. We determined that both doping portions worked well as the starting point of the graphitization. While the spontaneous vibration of the pillar deteriorated the image, the grain boundaries of the graphitized area, which can be seen as a contrast in the TEM image, are clearly distinguished from the amorphous region. A few particles remained at the original doping area, while the front of the graphite proceeded to the middle of the pillar. There the graphitizing velocity was roughly estimated to be 1 μm/h at 820 °C.

Such graphitization proceeded over the junction in the Y-branch structure, as shown in Fig. 5, where the iron catalyst was doped at the top of one of the side branches. Two solid-phase-crystallization events occurred, one at the graphitization that originated from the iron catalyst and the formation of SiC as a reaction with the substrate at the bottom of the pillar. The electron-diffraction pattern at the bottom area clearly suggested the formation of SiC, as indicated by white circle 1 in Fig. 5, where the Y-branch pillar was annealed for 1 h at 820 °C. The diffraction pattern of the intermediate position of the doped branch, indicated by white circle 2, as well as the intermediate position of another nondoped branch, indicated by white circle 3, has a clear innermost ring that originated from the graphite [0002] and its conjugated diffractions. These diffraction patterns were obtained by using selective area diffraction where the analyzed area was estimated to be about 200 nm. Thus, the solid phase graphitization of this Y-branch pillar crossed over the junction and propagated to the halfway point of the nondoped branch.

V. DISCUSSION

The growth mechanism of nanotube growth under the gas-phase condition[8] with the catalyst basically corresponded to the following steps: (1) the supplied source gas was adsorbed at the catalyst surface; (2) the decomposed material migrated toward the growing position through the catalyst surface; and (3) the decomposed fragment fed the nanotube growth. This means that the atom and/or molecular migration on the catalyst surface was essential to the nanotube growth.

However, there was no dynamic flow of mother material (amorphous carbon) around the iron catalyst, unlike the gas-phase growth of the nanotube. Another way that the graphitization could possibly have occurred was via a migration of the catalyst. The reaction on the catalyst is in equilibrium between the decomposing and crystallizing processes. Thus, the movement of the catalyst proceeded simultaneously to supplement new mother material and the production of graphite. However, the TEM image in Fig. 5 shows that none of the iron particles existed at the front of the graphitization. We think the graphitization of the amorphous carbon pillar was due to a homo-epitaxial growth based on the solid phase crystallization templated on the graphite. The Young's modulus of the annealed amorphous carbon pillar generally showed a lower value due to an increase of $sp2$ bonding, but some of graphitized carbon pillar showed a higher value Young's modulus than that of the as-grown pillar. If we take into account the mass reduction changing the Young's modulus, the graphitization appears to have increased the Young's modulus.

While we need further analysis of the graphitizing mechanism and an improvement of the growth technique, this ex-

periment was the first reported demonstration of a solid phase graphitization on a FIB-CVD amorphous carbon pillar. The samples obtained in this experiment were still thick from the viewpoint of nanotube applications, however, some of the beam-induced pillars[9–11] had much smaller diameters. The basic mechanism of graphitization that we demonstrated here is presumably applicable to such thinner amorphous carbon structures. In addition, graphitization with a single grain will probably be possible in a thinner carbon pillar, because the nucleation energy of the grain boundary will increase with decreases of the pillar diameter, thus, this is an artificially manipulated multi-wall nanotube. We think that combining this partial iron-doping technique with the beam-induced fine-pattern-formation technique will realize the position selective growth of nanotubes, which will open a new window of discovery in the development of nanoscale three-dimensional device architectures.

VI. SUMMARY

We demonstrated graphitization that began from an amorphous carbon pillar containing an iron catalyst, which was doped using ferrocene gas in FIB-CVD. The technique used for the graphitization of amorphous carbon is based on solid phase crystallization, where homo-epitaxial growth on a graphite template appeared to occur. The original shape of an as-grown structure survived the solid phase graphitization at 820 °C. This demonstration strongly suggests the possibility of position selective growth of nanotube and nanoscale three-dimensional electron devices.

[1]S. Matsui, T. Kaito, J. Fujita, M. Komuro, K. Kanda, and Y. Haruyama, J. Vac. Sci. Technol. B **18**, 3181 (2000).
[2]J. Fujita, M. Ishida, T. Sakamoto, Y. Ochiai, T. Kaito, and S. Matsui, J. Vac. Sci. Technol. B **19**, 2834 (2001).
[3]J. Fujita, M. Ishida, T. Ichihashi, T. Sakamoto, Y. Ochiai, T. Kaito, and S. Matsui, Jpn. J. Appl. Phys. (in press).
[4]N. Hamada, S. Sawada, and A. Oshiyama, Phys. Rev. B **45**, 6234 (1992).
[5]R. Martel, T. Schmidt, H. R. Shea, T. Hertel, and P. Avouris, Appl. Phys. Lett. **73**, 2447 (1998).
[6]S. J. Tans, A. R. M. Verschueren, and C. Dekker, Nature (London) **393**, 49 (1998).
[7]S. Iijima, J. Phys. Chem. **91**, 3466 (1987).
[8]S. Fan, M. Chapline, N. Franklin, T. Tomber, A. Cassel, and H. Dai, Science **283**, 512 (1999).
[9]I. Utke, P. Hoffmann, B. Dwir, K. Leifer, E. Kapon, and P. Doppelt, J. Vac. Sci. Technol. B **18**, 3168 (2000).
[10]A. J. DeMarco and J. Melngailis, J. Vac. Sci. Technol. B **17**, 3154 (1999).
[11]H. W. Koops, Jpn. J. Appl. Phys., Part 1 **33**, 7099 (1994).